



**HAL**  
open science

## A new cross section measurement of reactions induced by $^3\text{He}$ -particles on a carbon target

A. Pichard, J. Mrazek, M. Assié, M. Hass, M. Honusek, G. Lhersonneau, F. de  
Oliveira de Santos, M.G. Saint-Laurent, E. Simeckova

► **To cite this version:**

A. Pichard, J. Mrazek, M. Assié, M. Hass, M. Honusek, et al.. A new cross section measurement of reactions induced by  $^3\text{He}$ -particles on a carbon target. 2010. in2p3-00544574v1

**HAL Id: in2p3-00544574**

**<https://hal.in2p3.fr/in2p3-00544574v1>**

Preprint submitted on 8 Dec 2010 (v1), last revised 3 May 2011 (v2)

**HAL** is a multi-disciplinary open access archive for the deposit and dissemination of scientific research documents, whether they are published or not. The documents may come from teaching and research institutions in France or abroad, or from public or private research centers.

L'archive ouverte pluridisciplinaire **HAL**, est destinée au dépôt et à la diffusion de documents scientifiques de niveau recherche, publiés ou non, émanant des établissements d'enseignement et de recherche français ou étrangers, des laboratoires publics ou privés.

# A new cross section measurement of reactions induced by $^3\text{He}$ -particles on a carbon target

A. Pichard<sup>1</sup>, J. Mrázek<sup>2</sup>, M. Assié<sup>3</sup>, M. Hass<sup>4</sup>, M. Honusek<sup>2</sup>, G. Lhersonneau<sup>1</sup>, F. de Oliveira de Santos<sup>1</sup>, M.-G. Saint-Laurent<sup>1</sup>, and E. Šimečková<sup>2</sup>

<sup>1</sup> GANIL, CEA/DSM-CNRS/IN2P3, Caen, France

<sup>2</sup> Nuclear Physics Institute ASCR P.R.I., Řež, Czech Republic

<sup>3</sup> IPN, Université Paris-Sud - 11 - CNRS/IN2P3, Orsay, France

<sup>4</sup> Weizmann Institute, Rehovot, Israël

Received: date / Revised version: date

**Abstract.** The production of intense beams of light radioactive nuclei can be achieved at the SPIRAL2 facility using intense stable beams accelerated by the driver accelerator and impinging on light targets. The isotope  $^{14}\text{O}$  is identified to be of high interest for future experiments. The excitation function of the production reaction  $^{12}\text{C}(^3\text{He}, n)^{14}\text{O}$  was measured between 7 and 35 MeV. Results are compared with literature data. As an additional result, we report the first cross-section measurement for the  $^{12}\text{C}(^3\text{He}, \alpha+n)^{10}\text{C}$  reaction. Based on this new result, the potential in-target  $^{14}\text{O}$  yield at SPIRAL2 was estimated:  $2.4 \times 10^{11}$  pps, for 1 mA of  $^3\text{He}$  at 35 MeV. This is a factor 140 higher than the in-target yield at SPIRAL1.

**PACS.** 25.55.-e  $^3\text{H}$ ,  $^3\text{He}$  and  $^4\text{He}$ -induced reactions – 27.20.+n  $6 < A < 19$

## 1 Introduction

A collaboration between GANIL (France), Soreq Nuclear Research Center and Weizmann Institute (Israël) has been formed in order to study the production options for in-

---

*Send offprint requests to:* F. de Oliveira de Santos, e-mail francois.oliveira@ganil.fr

tense light radioactive ion beams at the future SPIRAL2 [1] facility in the framework of the European FP7 Preparatory Phase of SPIRAL2 [2,3]. The short-lived (71 s)  $^{14}\text{O}$  beam was identified to be of high interest for future experiments [4–7] and therefore options for his production have been studied in details. The reaction  $^{12}\text{C}(^3\text{He}, n)^{14}\text{O}$  was chosen for production because a carbon target is able to

sustain a very intense beam of  $^3\text{He}$ , up to 1 mAe. However, large discrepancies are observed in the various excitation functions available in the literature [8–12]. Consequently, we decided to perform a new measurement of this cross section. The residual activity of thin carbon foils irradiated by the  $^3\text{He}$  primary beam was used to measure the production rate. A special attention has been given to the measurement normalisation. Apart from a standard current measurement, we have used an activation monitor: aluminium and cobalt foils irradiated simultaneously by the primary beam. As a matter of fact, excitation functions for  $^{27}\text{Al}(^3\text{He}, 2\text{p})^{28}\text{Al}$  and  $^{59}\text{Co}(^3\text{He}, \text{x})$  reactions are well known and allow an extra check of the primary beam intensity. One of the complementary results of this experiment is the first measurement of the excitation function of the  $^{12}\text{C}(^3\text{He}, \alpha+n)^{10}\text{C}$  reaction.

## 2 Experimental setup

The experiment took place at NPI (Nuclear Physics Institute, Řež, Czech Rep.). The isochronous cyclotron U-120M can deliver  $^3\text{He}^{2+}$  beams at energies up to 38 MeV. Measurements have been performed with two different beam energies: 38 and 24.5 MeV. Intermediate irradiation energies were obtained by means of energy degraders foils made of Aluminium disposed on a rack placed in front of the target. In figure 1, a scheme of the irradiation station is presented. The targets are composed of three stacked disks of 1 cm radius: a  $3\text{-}\mu\text{m}$  thick Mylar disk, the thin carbon target ( $75\ \mu\text{m}$ ,  $1.1\ \text{g}\cdot\text{cm}^{-3}$ ) and a  $10\text{-}\mu\text{m}$  thick aluminium disk. The carbon target wrapping prevented  $^{14}\text{O}$  to escape

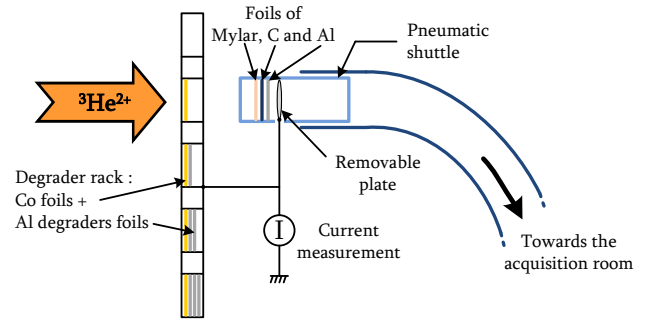
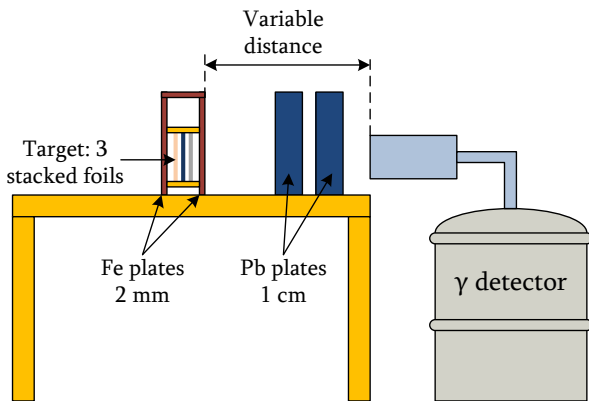


Fig. 1. Schematic view of the irradiation station

in the volatile form  $\text{C}^{14}\text{O}$ . Moreover, the aluminium disk stopped the reaction products having enough energy to leave the carbon target. A plate located at the back of the target stopped the primary beam. The foils isotopic purity was 99.9 %.

The stacks were irradiated during 200 s, i.e. three times the  $^{14}\text{O}$  lifetime (71 s), to reach near activity saturation. Then, the target was transported from the irradiation station to the low background acquisition room via a pneumatic transport system. The scheme shown in Fig. 2 describes the acquisition setup. The target was placed along the axis of a HPGe detector used as  $\gamma$  spectrometer. The target was shielded with 2 cm of lead and 2 mm of iron in order to reduce the flux of the very intense 511 keV gamma line relatively to the main gamma line of  $^{14}\text{O}$  at 2.312 MeV. The annihilation 511 keV  $\gamma$ -ray originates from the decay of  $^{14}\text{O}$ ,  $^{11}\text{C}$  and  $^{13}\text{N}$  reaction products. Three distances between the target and the detector were used in order to keep the counting rate at an acceptable level. The detector was calibrated in the same configurations with  $^{152}\text{Eu}$  and  $^{90}\text{Nb}$  radioactive sources. Each target counting



**Fig. 2.** Scheme of the acquisition setup placed in the low background room

lasted 300 s. The Co foils  $\gamma$ -counting was carried out until several weeks after irradiation due to the long life-time of some of the elements produced. Their counting rate being consequently lower, the measurements were performed in a lead castle in order to limit the natural background.

### 3 Data Evaluation

Basic nuclear data and Q-values of the contributing reactions are collected in table 1. The 1238 keV  $^{56}\text{Co}$   $\gamma$ -line was not used because it was polluted by another line from the acquisition room background. The number of incident particles was obtained by real time measurement of the current collected on a metallic plate placed at the back of the target and on the degrader rack. Simultaneous irradiation of aluminium and cobalt foils by the beam allowed a check of this measurement:

- The cross section for  $^{27}\text{Al}(^3\text{He}, 2p)^{28}\text{Al}$  is known to good accuracy [13]. The  $^{28}\text{Al}$  (2.2 m) yield measured in the 10- $\mu\text{m}$  aluminium foils placed at the back of the car-

bon target allowed us to calculate the  $^3\text{He}$  integral intensity received by the target at each irradiation.

- The excitation functions of reactions induced by  $^3\text{He}$  on cobalt being well known too [14–19], a stack of 3  $\mu\text{m}$ -thick cobalt foils placed on the degrader rack also allowed for checking the normalisation.

The cross-section uncertainties have been estimated by summing quadratically the uncertainties of the different contributing processes:

- The dead time of counting is monitored by a pulse generator. Its accuracy is always better than 1 %.
- Accuracies on branchings per decay of the monitored  $\gamma$ -rays are given in table 1.
- The accuracy on the efficiency of the  $\gamma$  detector, including transmission through the lead plates, is the main contribution to the total error. It is estimated to be about 6 % for the 2313 keV line of  $^{14}\text{O}$  and the 1779 keV line of  $^{28}\text{Al}$ , 10 % for the  $\gamma$ -rays from the cobalt foils and about 25 % for the 718 keV line of  $^{10}\text{C}$ .
- The number of target atoms in each disk is deduced by weighting. The accuracy is about 3 % for the aluminium and carbon disks and about 10 % for the cobalt foils.
- The accuracy of the primary beam intensity is estimated to 5 % from the current measurement device. It is confirmed by the evaluation of activity generated by the beam in Aluminium foils, see section 4.4.1.

### 4 Results

Table 2 shows the measured cross-sections obtained for the  $^{12}\text{C}(^3\text{He}, n)^{14}\text{O}$  and  $^{12}\text{C}(^3\text{He}, \alpha+n)^{10}\text{C}$  reactions and

**Table 1.** Investigated nuclear reactions induced in C, Al and Co by  $^3\text{He}$  particles irradiation

Foil	Isotope	Half-life	$E_\gamma$ (keV)	$I_\gamma$ (%)	Reactions	Q (MeV)
$^{12}\text{C}$	$^{14}\text{O}$	70.61 s	2312.6	99.388(11)	$^{12}\text{C}(^3\text{He}, \text{n})^{14}\text{O}$	1.4
	$^{10}\text{C}$	19.26 s	718.3	98.53(2)	$^{12}\text{C}(^3\text{He}, \alpha+\text{n})^{10}\text{C}$	-11.3
					$^{12}\text{C}(^3\text{He}, ^3\text{He}+2\text{n})^{10}\text{C}$	-31.8
					$^{12}\text{C}(^3\text{He}, 2\text{d}+\text{n})^{10}\text{C}$	-35.1
					$^{12}\text{C}(^3\text{He}, 2\text{p}+3\text{n})^{10}\text{C}$	-39.6
$^{27}\text{Al}$	$^{28}\text{Al}$	2.24 m	1779.0	100	$^{27}\text{Al}(^3\text{He}, 2\text{p})^{28}\text{Al}$	$7.0 \times 10^{-3}$
$^{59}\text{Co}$	$^{60}\text{Cu}$	23.7 m	826.1	21.7(11)	$^{59}\text{Co}(^3\text{He}, 2\text{n})^{60}\text{Cu}$	-5
			1791.6	45.4(23)		
	$^{61}\text{Cu}$	3.33 h	283.0	12.2(3)	$^{59}\text{Co}(^3\text{He}, \text{n})^{61}\text{Cu}$	6.6
			656.0	10.77(18)		
	$^{56}\text{Co}$	77.23 d	846.8	100	$^{59}\text{Co}(^3\text{He}, 2\text{n}+\alpha)^{56}\text{Co}$	-9.8
			1037.8	13.99(10)	$^{59}\text{Co}(^3\text{He}, 2\text{t})^{56}\text{Co}$	-21.2
	$^{57}\text{Co}$	271.7 d	122.1	85.60(17)	$^{59}\text{Co}(^3\text{He}, \alpha+\text{n})^{57}\text{Co}$	1.5
			136.5	10.68(8)	$^{59}\text{Co}(^3\text{He}, \text{d}+\text{t})^{57}\text{Co}$	-16
					$^{59}\text{Co}(^3\text{He}, \text{n}+\text{p}+\text{t})^{57}\text{Co}$	-18.3
					$^{59}\text{Co}(^3\text{He}, ^3\text{He}+2\text{n})^{57}\text{Co}$	-19
					$^{59}\text{Co}(^3\text{He}, \text{n}+2\text{d})^{57}\text{Co}$	-22.3
					$^{59}\text{Co}(^3\text{He}, 2\text{n}+\text{p}+\text{d})^{57}\text{Co}$	-24.5
	$^{58\text{m}+g}\text{Co}$	70.86 d	810.8	99.45(1)	$^{59}\text{Co}(^3\text{He}, \alpha)^{58}\text{Co}$	10.1
					$^{59}\text{Co}(^3\text{He}, \text{p}+\text{t})^{58}\text{Co}$	-9.6
$^{59}\text{Co}(^3\text{He}, ^3\text{He}+\text{n})^{58}\text{Co}$					-10.4	
$^{59}\text{Co}(^3\text{He}, 2\text{d})^{58}\text{Co}$					-13.7	
$^{59}\text{Co}(^3\text{He}, \text{n}+\text{p}+\text{d})^{58}\text{Co}$					-15.9	
$^{59}\text{Co}(^3\text{He}, 2\text{n}+2\text{p})^{58}\text{Co}$					-18.2	

for the  $^{27}\text{Al}(^3\text{He}, 2\text{p})^{28}\text{Al}$  monitor reaction. Each target was irradiated and counted twice to reduce uncertainties. The values  $\sigma$  give the measured cross-section for each irradiation, which are subsequently combined to obtain the resultant mean value  $\sigma_r$  presented in the table. The energy degradation  $\Delta E$  inside the target and the mean primary beam energy  $\langle E \rangle$  were calculated with the code LISE++ [20] using the Ziegler [21] low-energy model for both C and Al foils. A measurement with a carbon target thick enough to stop fully the primary beam was done at 36 MeV. This measurement directly gives the thick target yield. The cross-section integrated over the whole energy range (and folded with stopping power) was thus calculated and is presented on the last line of the table 2.

#### 4.1 Comparison of cross-sections for $^{14}\text{O}$

Figure 3 shows a comparison of our measurement with literature for the  $^{12}\text{C}(^3\text{He}, \text{n})^{14}\text{O}$  reaction. Three authors report measurements at low energy (2 to 12 MeV).

The shape and normalisation of the excitation functions presented by Cirilov *et al.* [8] and by Hahn and Ricci [9] seem to be consistent. They show a 15 mb maximum at 5 MeV. The excitation function presented by Osgood *et al.* [10] has quite a similar structure but, while the absolute value is comparable for energies lower than 4 MeV, it rises to reach a 35 mb maximum at 7 MeV. The only measurement at higher energies was done by Singh [11] who, however, was on relative scale. He normalised his values to those of Osgood *et al.* The excitation function decreases smoothly from 27 mb at 6 MeV to 12 mb at

30 MeV. We also display the excitation function given by the nuclear model code system TALYS [22]. The code has been forced to take into account only the contribution of the ground state since all the excited states would decay by  $^{14}\text{O}^* \rightarrow ^{13}\text{N} + \text{p}$ . Our only measurement at low energy (7 MeV) places sigma between the values given by Osgood *et al.*, on the one hand, and those given by Cirilov *et al.* and by Hahn and Ricci, on the other hand. It presents a large energy spread (4 MeV), so that it is not possible to directly compare it with those values. At higher energies, our values are a factor 4 lower than those of Singh.

#### 4.2 In-target yield of $^{14}\text{O}$

The thick-target yields are obtained by folding the energy loss of the primary beam in the target with the excitation functions of the  $^{12}\text{C}(^3\text{He}, \text{n})^{14}\text{O}$  reaction. Figure 4 shows a comparison of these yields with the target saturation activity measured by Nozaki and Iwamoto [12] (full dots). The dashed and short-dashed lines are calculated from the excitation function given by Singh and the code TALYS, respectively. The highest solid line is calculated with data from Osgood *et al.* for energies between 1.6 and 11.5 MeV and our data from 14.4 to 35.3 MeV. The lowest solid line is calculated with data from Cirilov *et al.* for energies between 1.55 and 5.76 MeV, data from Hahn and Ricci for energies between 6 and 12.2 MeV and our data between 14.4 to 35.3 MeV. The value calculated by integrating Singh's data up to 30 MeV,  $5.7 \times 10^{11}$  pps, could indicate he used a too high value for normalisation. The target saturation activities measured by Nozaki and

**Table 2.** Measured cross-sections for the  $^{12}\text{C}(^3\text{He}, \text{n})^{14}\text{O}$ ,  $^{12}\text{C}(^3\text{He}, \alpha+\text{n})^{10}\text{C}$  and  $^{27}\text{Al}(^3\text{He}, 2\text{p})^{28}\text{Al}$  reactions

$^{12}\text{C}$		$^{27}\text{Al}$		$^{12}\text{C}(^3\text{He}, \text{n})^{14}\text{O}$		$^{12}\text{C}(^3\text{He}, \alpha+\text{n})^{10}\text{C}$		$^{27}\text{Al}(^3\text{He}, 2\text{p})^{28}\text{Al}$	
$\langle E \rangle / \Delta E$ (MeV)	$\langle E \rangle / \Delta E$ (MeV)	$\sigma$ (mb)	$\sigma_r$ (mb)	$\sigma$ (mb)	$\sigma_r$ (mb)	$\sigma$ (mb)	$\sigma_r$ (mb)	$\sigma$ (mb)	$\sigma_r$ (mb)
7.2 / 4.1	4.2 / 1.7	19(2)	18(2)	-	-	24(2)	23(2)		
		17(2)		-		23(2)			
14.4 / 2.4	12.8 / 0.8	7.2(7)	7.3(7)	-	-	184(15)	186(15)		
		7.4(7)		-		187(15)			
18.0 / 2.0	16.7 / 0.7	5.6(6)	5.5(6)	-	1(1)	274(22)	265(22)		
		5.4(6)		1(1)		255(42)			
20.0 / 1.9	18.8 / 0.6	3.9(4)	3.8(4)	2(1)	1.9(7)	217(18)	221(18)		
		3.8(4)		1.8(7)		224(18)			
20.6 / 1.8	19.4 / 0.6	3.8(4)	3.8(3)	2.2(7)	2.4(7)	222(18)	227(18)		
		3.8(4)		3(1)		232(19)			
26.3 / 1.5	25.3 / 0.5	3.0(3)	3.0(3)	11(3)	11(3)	161(14)	160(13)		
		3.1(3)		11(3)		158(13)			
28.3 / 1.4	27.4 / 0.5	2.5(3)	2.5(3)	11(3)	12(3)	131(11)	131(11)		
		2.5(3)		12(3)		132(11)			
29.7 / 1.3	28.8 / 0.4	1.8(2)	1.8(2)	10(3)	10(3)	121(10)	120(10)		
		1.8(2)		9(3)		120(10)			
34.9 / 1.2	34.1 / 0.4	1.6(2)	1.7(2)	13(4)	13(3)	97(8)	98(8)		
		1.7(2)		13(4)		100(8)			
35.3 / 1.2	34.6 / 0.4	1.3(2)	1.3(2)	13(4)	12(3)	96(8)	96(8)		
		1.3(2)		13(4)		95(8)			
		1.4(2)		11(3)		98(8)			
18 / 18	-	2.9(3)	2.9(3)	-	-	-	-		
		2.9(3)		-					

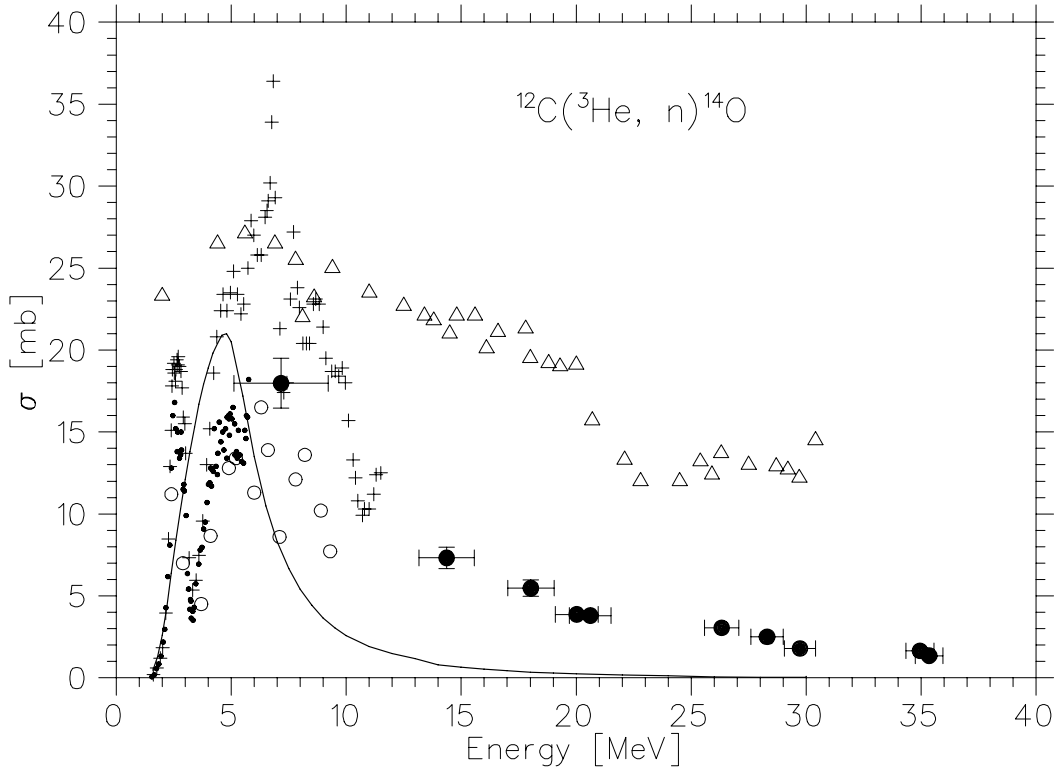


**Fig. 3.** Excitation functions for the  $^{12}\text{C}(^3\text{He},n)^{14}\text{O}$  reaction. ●: Our data, ○: Hahn and Ricci, +: Osgood *et al.*, Δ: Singh, ●: Cirilov *et al.*, thick line: calculated by TALYS.

Iwamoto are not consistent with low-energy cross section measurements made by the other authors. Thus, our estimate of the in-target yield at SPIRAL2, read from the solid curves, ranges from  $1.8$  to  $2.4 \times 10^{11}$  pps for 1 mA of  $^3\text{He}$  at 35 MeV.

#### 4.3 Cross-section for the production of $^{10}\text{C}$

A complementary result of this experiment is the measurement of the  $^{10}\text{C}$  production cross-section. To our knowl-

edge, this is the first report of experimental data for this reaction. In the energy range used, the reaction mainly contributing to the production is  $^{12}\text{C}(^3\text{He}, \alpha+n)^{10}\text{C}$  (see the Q-values in table 1). In figure 5, they are compared with values given by TENDL-09 [23,24], a nuclear data library which provides the output of the TALYS code. The measured excitation function starts to increase at about 20 MeV to reach 12 mb between 25 and 35 MeV.

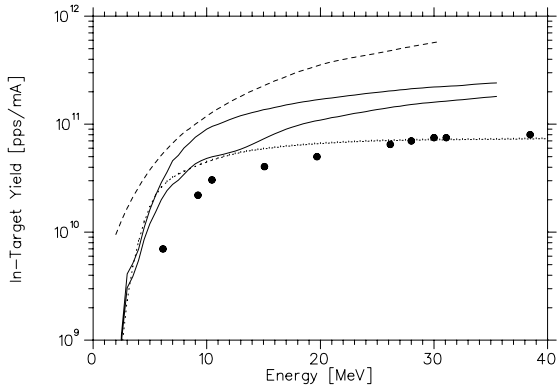


**Fig. 4.** Comparison of the thick target production yields from the  $^{12}\text{C}(^3\text{He},n)^{14}\text{O}$  reaction as a function of the primary beam energy. Dashed line: Singh, short dashed line: TENDL-09 data base, solid lines: lower and upper estimates using our and combined data. Full dots are Nozaki and Iwamoto target saturation activity measurements.

#### 4.4 Monitor reactions

A special care was taken for the normalisation. For this goal, aluminium and cobalt foils were irradiated simultaneously with the targets to monitor the primary beam intensity.

##### 4.4.1 Aluminium foils

The aluminium foil was the last disk of the target stack. A part of  $^{28}\text{Al}$  produced via  $^{27}\text{Al}(^3\text{He}, 2p)^{28}\text{Al}$  had enough kinetic energy to escape from the Al disk. This fraction was calculated with the ISOL Catcher utility [25] of the code LISE++. This fraction depends of the primary beam energy. At 34.6 MeV, it represents 23.5 % of the total pro-

duction. In figure 6, our data (full dots) are compared to the measurement made by Frantsvog *et al.* (empty squares) and with the simulation data base TENDL-09 (dashed line). Frantsvog *et al.* used thicker targets so that their energy spread is higher than ours. Since we cannot compare directly their values to ours, we have interpolated our cross-section versus energy and subsequently integrated on the corresponding energy range. The resultant values are represented by empty triangles on the graph. It appears that the agreement between our measurements and Frantsvog *et al.* is good, comforting us in the validity of the normalisation factor obtained by measuring the charge.

##### 4.4.2 Cobalt foils

Cobalt foils allowed us monitoring the primary beam intensity by the well known cross-sections of the following reactions :  $^{59}\text{Co}(^3\text{He},2n)^{60}\text{Co}$ ,  $^{59}\text{Co}(^3\text{He}, n)^{61}\text{Co}$ ,  $^{59}\text{Co}(^3\text{He},$

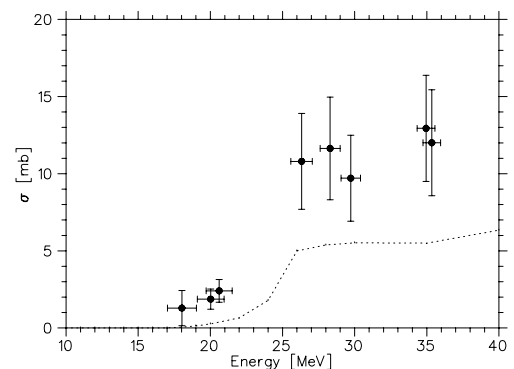


**Fig. 5.** Excitation functions for the  $^{12}\text{C}(^3\text{He}, \alpha+n)^{10}\text{C}$  reaction. ●: Our data, dashed line: TENDL-09 data base.

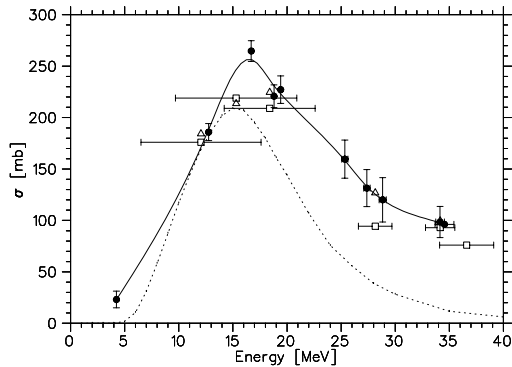


**Fig. 6.** Excitation function for the  $^{27}\text{Al}(^3\text{He}, 2\text{p})^{28}\text{Al}$  beam monitor reaction;  $\bullet$ : our data,  $\square$ : Frantsvog *et al.*,  $\triangle$ : our data averaged on the energy spread for comparison with the ones of Frantsvog *et al.*, dashed line: TENDL-09 data base, solid line: spline interpolation of our data

$x)^{56}\text{Co}$ ,  $^{59}\text{Co}(^3\text{He}, x)^{57}\text{Co}$  and  $^{59}\text{Co}(^3\text{He}, x)^{58}\text{Co}$ . The proportion of reaction fragments leaving the Co foil is taken into account. It was determined that this proportion never exceeds 10 % at 21.3 MeV and 16 % at 38 MeV of the total production. Our results are shown in the table 3. They were compared with those of Fenyvesi *et al.* [14], Nagame *et al.* [15], Szelecsényi *et al.* [16], Michel and Galas [17], Homma and Murakami [18] and Kondratyev *et al.* [19]. All data are not shown here for clarity. It appeared that our values are systematically higher by 20 % than those given by these authors. Wrong normalisation of the primary beam intensity would contradict the excellent results obtained with Al foils. Part of the discrepancy could be ascribed to the thickness of the Co foils which has a 10 % uncertainty. In all cases, the activation of cobalt foils

confirms that no large error was committed in the primary beam intensity normalisation.

## 5 Outlook

A  $^{14}\text{O}$  beam is currently available at GANIL within the SPIRAL1 facility. It is produced via the fragmentation of a  $^{16}\text{O}$  primary beam in a graphite target. An intensity of  $3.2 \times 10^5$  particles per second (pps) is available for experiments in an energy range from 3.2 up to 12.5 MeV/A [26]. With the new facility SPIRAL2, the intense  $^3\text{He}$  (1 mA / 43.5 MeV) beam delivered by the LINAC driver offers opportunities to raise the available  $^{14}\text{O}$  beam intensity. The present measurement of the  $^{12}\text{C}(^3\text{He}, n)^{14}\text{O}$  cross-section clarifies discrepancies among thick-target yields reported in the past. Based on this new result, we can estimate the potential in-target  $^{14}\text{O}$  yield:  $2.4 \times 10^{11}$  pps, for 1 mA of  $^3\text{He}$  at 35 MeV. This is a factor 140 higher than the in-target yield at SPIRAL1. Preliminary simulations of the thermal conditions did show that the maximal intensity the production target can withstand is indeed close to 1 mA. A production system is currently being designed at GANIL and simultaneously more precise thermal simulations will be carried out with the designed target.

## 6 Acknowledgement

We thank the Řež cyclotron and technical crew for delivering the  $^3\text{He}$  beam and for the nice working conditions. We are also grateful to Dr. Lebeda for providing us the  $^{90}\text{Nb}$  calibration source. This work has been supported by

**Table 3.** Measured cross-section for  $^3\text{He}$ -induced reactions on  $^{59}\text{Co}$ 

$\langle E \rangle$ (MeV)	$\Delta E$ (MeV)	$\sigma$ (mb) of $^{59}\text{Co}(^3\text{He},x)$ reactions				
		$^{60}\text{Cu}$	$^{61}\text{Cu}$	$^{56}\text{Co}$	$^{57}\text{Co}$	$^{58m+g}\text{Co}$
21.3	0.4	112(15)	8(1)	10(1)	126(16)	28(5)
			8(1)	9(1)	111(14)	25(4)
35.8	0.3			75(10)	51(9)	302(42)
				58(9)	36(8)	250(34)
				79(11)	50(10)	332(45)

the IN2P3 - ASCR, by the European Community FP7 - Capacities - SPIRAL2 Preparatory Phase N $^{\circ}$  212692, and by the Région Basse Normandie for a PhD thesis (A.P.).

## References

1. GANIL - SPIRAL2 - GANIL WEB PRO USERS, <http://pro.ganil-spiral2.eu/>.
2. G. Lhersonneau, A. Pichard, M. Saint Laurent, F. De Oliveira Santos, M. Hass, T.Y. Hirsh, *et al.*, Rapport Européen, WP7.1 Milestone 7.1.1, (2009).
3. M.G. Saint Laurent, A. Pichard, G. Lhersonneau, F. De Oliveira Santos, F. Pellemoine, P. Delahaye, *et al.*, International Symposium on Exotic Nuclei (EXON), Sochi, Russian Federation (2009).
4. J.T. Burke, P.A. Vetter, S.J. Freedman, B.K. Fujikawa, W.T. Winter, *Phys. Rev. C.* 74 (2006) 025501-5.
5. M. Gaelens, J. Andrzejewski, J. Camps, P. Decrock, M. Huyse, K. Kruglov, *et al.*, *EPJ A* 11 (2001) 413-420.
6. D.W. Bardayan, M.S. Smith, *Phys. Rev. C.* 56 (1997) 1647.
7. I. Stefan, F. De Oliveira Santos, M.G. Pellegriti, M. Angeliq, J.C. Dalouzy, F. de Grancey, *et al.*, International Conference-PROCON 2007, Lisbon (Portugal), AIP, (2007) 205-210.
8. S.D. Cirilov, J.O. Newton, J.P. Schapira, *Nuclear Physics.* 77 (1966) 472-476.
9. R.L. Hahn, E. Ricci, *Phys. Rev.* 146 (1966) 650.
10. D.R. Osgood, J.R. Patterson, E.W. Titterton, *Nuclear Physics.* 60 (1964) 503-508.
11. J. Singh, *Nuclear Physics A.* 155 (1970) 443-452.
12. T. Nozaki, M. Iwamoto, *Radiochimica Acta.* 29 (1981) 57-59.
13. D.J. Frantsvog, A.R. Kunselman, R.L. Wilson, C.S. Zaidins, C. Détraz, *Phys. Rev. C.* 25 (1982) 770.
14. A. Fenyvesi, F. Tárkányi, S.-. Heselius, *NIM B.* 222 (2004) 355-363.
15. Y. Nagame, Y. Nakamura, M. Takahashi, K. Sueki, H. Nakahara, *Nuclear Physics A.* 486 (1988) 77-90.
16. F. Szelecsényi, Z. Kovács, K. Suzuki, K. Okada, T. Fukumura, K. Mukai, *NIM B.* 222 (2004) 364-370.
17. R. Michel, M. Galas, *Nuclear Physics A.* 404 (1983) 77-92.
18. Y. Homma, Y. Murakami, *Bull.of the Chemical Soc.of Japan.* 50 (1977) 1251.

19. S. Kondratyev, Y. Lobach, V. Sklyarenko, Ukrainskii Fizichnii Zhurnal. 43 (1998) 5.
20. O. Tarasov, D. Bazin, NIM B. 266 (2008) 4657-4664.
21. U. Littmark, J.F. Ziegler, Handbook of range, distributions for energetic ions in all elements, Pergamon Press, 1980.
22. TALYS, <http://www.talys.eu/home/>.
23. TENDL-2009 - TALYS, <http://www.talys.eu/tendl-2009/>.
24. A.J. Koning, D. Rochman, to be published. JEFF-DOC 1310 (2009).
25. LISE++ : a simulation of fragment separators - Last modifications, <http://groups.nsl.msu.edu/lise/changes.html>.
26. Spiral beams - GANIL WEB PRO USERS, <http://pro.ganil-spiral2.eu/users-guide/accelerators/spiral-beams>.